ARTICLE

Short-Wavelength Electroluminescence from Single-Walled Carbon Nanotubes with High Bias Voltage

Norihito Hibino,[†,‡] Satoru Suzuki,[‡] Hiroyuki Wakahara,[†,‡] Yoshihiro Kobayashi,[‡] Tetsuya Sato,[†] and Hideyuki Maki[†,*]

[†]Department of Applied Physics and Physico-Informatics, Faculty of Science and Technology, Keio University, Hiyoshi, Yokohama 223-8522, Japan, and [‡]NTT Basic Research Laboratories, Nippon Telegraph and Telephone Corporation, Morinosato-Wakamiya, Atsugi 243-0198, Japan

ABSTRACT Short-wavelength electroluminescence (EL) emission is observed from unipolar and ambipolar carbon nanotube field-effect transistors (CNFETs) under high bias voltage. EL measurements were carried out with an unsuspended single-walled carbon nanotube (SWNT) in high vacuum to prevent the oxidation damage induced by current heating. Short-wavelength emission under high bias voltage is obtained because of the Schottky barrier reduction and the electric field increase in a SWNT. The simultaneous measurements of transport and EL spectra revealed the excitation mechanism of impact excitation or electron and hole injection dependent on the conduction type of unipolar or ambipolar characteristics. In addition to the EL emission, blackbody radiation was also observed in a p-type CNFET. Taking into account the device temperature estimated from blackbody radiation, the contribution of impact excitation and thermal effect to the exciton production rate was evaluated.

KEYWORDS: carbon nanotubes · electroluminescence · blackbody radiation · field-effect transistors · impact excitation · electron and hole injection · thermal effect

The carbon nanotube field-effect transistor (CNFET) is a promising nanoscale device due to the quasi-one-dimensional structure and the unique electronic properties of carbon nanotubes. Moreover, CNFETs are also expected to be utilized for optoelectronic devices because near-infrared (NIR) electroluminescence (EL) due to the recombination of excitons or free carriers is demonstrated in CNFETs with ambipolar[1−7] and unipolar[5,8] characteristics when applying bias voltage. (Quite recently, phonon-assisted EL in the visible region has also been demonstrated in metallic carbon nanotubes and graphenes.)[9] In the NIR EL from the CNFET, three mechanisms of excitations: (i) electron and hole injection in ambipolar CNFETs;[1−3,7] (ii) impact excitation in unipolar and ambipolar CNFETs;[4−6,8] and (iii) thermal excitation in quasimetallic CNFETs,[10,11] have been proposed.

The NIR EL wavelength due to excitons and free carriers in a semiconducting single-walled carbon nanotube (SWNT) is determined by the band gap,[12] which is inversely proportional to the diameter of the SWNT. In photoluminescence (PL) from SWNTs, a short-wavelength (~0.8 μm) emission can be obtained because the wide band gap SWNTs can be easily excited by using an short-wavelength excitation light.[12−17] In EL, however, only the longer wavelength (>~1.5 μm) emission has been reported due to the difficulty of electrically exciting the wide band gap SWNT.[1−8] In the electron and hole injection mechanism, it is not easy for the wide band gap SWNTs to inject sufficient electrons and holes to observe the EL emission due to the large height and width of the Schottky barriers for the wide band gap SWNTs.[18] In addition, in the impact excitation mechanism, excitation energy to create an exciton is high for the wide band gap SWNTs.[4,19−21] Therefore, the EL of these mechanisms is hard to obtain for the wide band gap SWNTs. For the short-wavelength EL emission, however, applying high bias voltage is an effective solution. At high bias voltage, the Schottky barrier height and width are reduced, and electrons and holes can be sufficiently injected to the wide band gap SWNTs. In addition, high bias voltage increases the accelerating field defined by the voltage drop and makes it possible to increase the impact excitation rate in the wide band gap SWNTs.[4,8,18] However, SWNTs easily break down by applying high bias voltage due to the oxidation induced by current heating.[22−24] Therefore, EL at a high bias voltage has not been demonstrated despite the expectation of the short-wavelength emission. In this study, we constructed an EL measurement

*Address correspondence to maki@appi.keio.ac.jp.

Received for review October 21, 2010 and accepted December 20, 2010.

Published online January 04, 2011
10.1021/nn1028373

© 2011 American Chemical Society

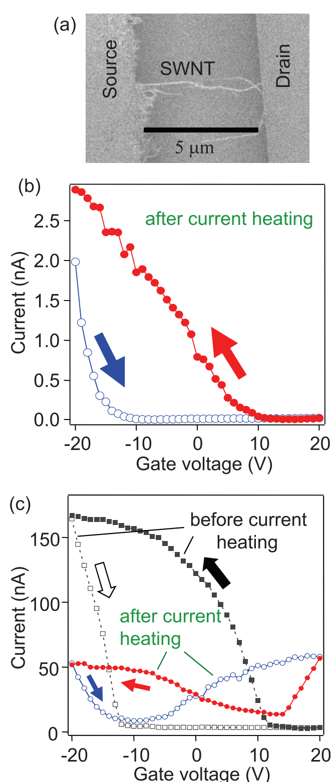

Figure 1. (a) Scanning electron microscope image of the CNFET device. (b) Gate voltage V_{gs} dependence of the current I_{ds} at the drain source voltage V_{ds} = 1 V for the device that keeps the p-type unipolar characteristic after current heating. Arrows indicate the positive (blue open circles) and negative (red solid circles) sweep direction of V_{gs}. (c) V_{gs} dependence of I_{ds} at V_{ds} = 1 V for the device that converted from the unipolar to ambipolar characteristic before (black squares) and after (blue and red circles) current heating. Arrows indicate the sweep direction of V_{gs}.

system, in which the electrical and EL measurements could be carried out in high vacuum to prevent current-induced oxidation. In addition, we used SWNTs lying on the substrate, *i.e.*, unsuspended carbon nanotubes, to dissipate heat to the substrate.[25] Using these techniques, we observed short-wavelength EL from p-type unipolar and ambipolar CNFETs at high bias voltage. The excitation mechanisms of carriers in EL emission were also investigated by the simultaneous measurements of transport and EL spectra. In addition to the EL emission, blackbody radiation was observed in a p-type CNFET. Taking into account the device temperature estimated from the blackbody radiation, we evaluated the contribution of impact excitation and thermal effect on the exciton production rate.

As-fabricated CNFETs exhibit a p-type unipolar characteristic at low bias voltage because the work function of Pd electrodes is high.[26,27] In this study, before the EL measurement, we applied high bias voltage (>5 V) to the devices and measured the gate voltage V_{gs} dependence of the current (I_{ds}) to investigate the electric properties at high bias voltage. During high-voltage application, two types of CNFETs exist: one is a device that maintains the p-type unipolar characteristic at high voltage (Figure 1b), and the other is the device converted from an unipolar to an ambipolar characteristic (Figure 1c). These unipolar or ambipolar characteristics are maintained after removal of the high voltage. Similar conversion was experimentally reported in the CNFETs using the electrical contact with the intermediate work-function metal of Ti and the high work-function metal of Pd.[7,30] The conversion in the CNFETs with the high work-function metal was previously understood by: (i) the Fermi level shift from the vicinity of the valence band top to the center of the band gap[28] or (ii) a charge transfer between the nanotubes and the water/oxygen redox couple.[29] In the first mechanism (i), it was theoretically explained that the Fermi level of the high work-function metal of Au can be strongly pinned at the center of the SWNT band gap when strong metal−SWNT bonds are formed at the interface.[28] In the second mechanism (ii), it was experimentally determined that the dominant effect for the ambipolar/unipolar conversion is linked to a charge transfer between the nanotubes and the water/oxygen redox couple and that the accumulation of negative charges changes the band-bending situation and thus limits electron injection.[29] However, it is not clear which mechanism is responsible to the present case, and further investigation is needed.

Figure 2a shows the typical EL spectra from the p-type unipolar device, which keeps the p-type characteristic after current heating, as a function of the bias voltage V_{ds} at $V_{gs} = -20$ V (Figure 2a). The EL emission is clearly observed, and the emission intensity is increased with increasing V_{ds}. These emissions consist of a single peak with a tail at the higher energy side. The emission peak energy (wavelength) is ~1.06 eV (~1.17 μm), which is consistent with the E_{11} excitonic transition estimated from the diameter ($d \sim 1.0$ nm) obtained by the atomic force microscopy (AFM) measurement.[31] The emission peak shifts slightly to higher energy with increasing V_{ds}. The V_{ds} dependence of I_{ds} and the EL intensity at $V_{gs} = -20$ V are shown in Figure 2b. The EL intensity is defined as the integrated peak intensity with background subtraction. At low V_{ds}, I_{ds} increases nonlinearly with increasing V_{ds} due to the reduction of the Schottky barrier height and width with increasing V_{ds}. I_{ds} linearly increases at the middle bias voltage of 8 V < V_{ds} < 16 V and saturates at a high bias voltage of V_{ds} > 16 V due to optical phonon scattering of electrons.[4,27,32,33] In previous studies, the current saturation due to optical phonon scattering was observed from several μA to more than 10 μA,[4,27,32,33] which is consistent with our result for the saturated I_{ds} (~7 μA). Although the EL emission was not observed at V_{ds} < 11 V, the EL intensity rapidly increased with increasing V_{ds} at V_{ds} > 11 V. By comparison between the EL and the current result in Figure 2b, the EL intensity exhibits exponential dependence on I_{ds} (Figure 2c).

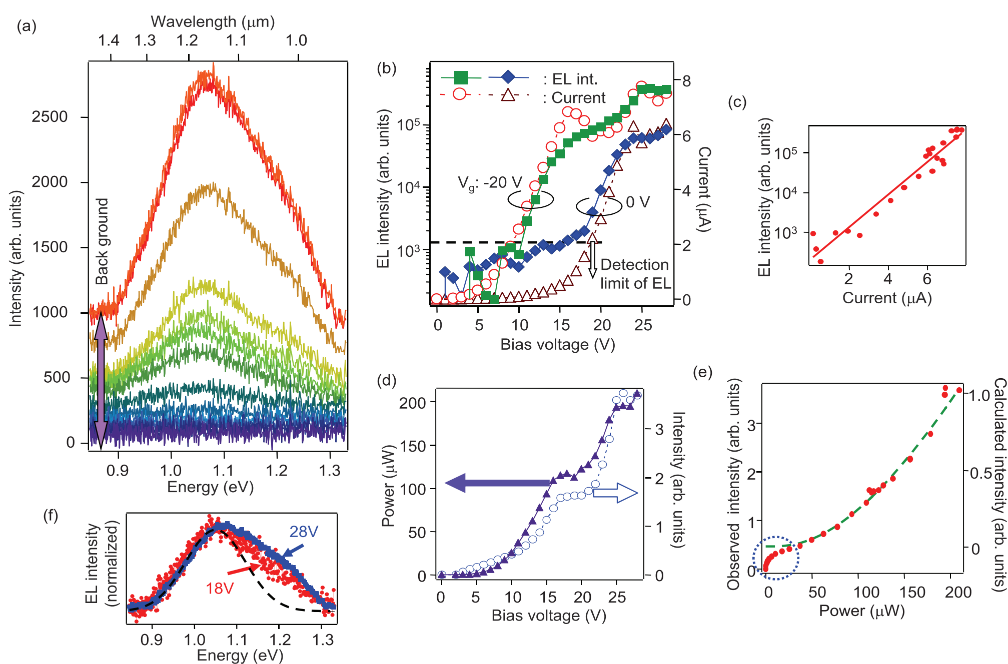

Figure 2. (a) EL spectra from the p-type unipolar device as a function of V_{ds} at V_{gs} = −20 V and V_{ds} = 0−28 V with steps of 2 V. Arrow indicates the background intensity at a wavelength of 1.45 μm for the EL spectrum at V_{ds} = 28 V. (b) V_{ds} dependence of I_{ds} (open circles and triangles) and EL intensity (solid squares and diamonds) at V_{gs} = −20 and 0 V, respectively. The detection limit of the EL intensity is indicated by the black broken line. (c) The EL intensity *vs* I_{ds} at V_{gs} = −20 V. The solid line indicates the line fitting for this result. (d) V_{ds} dependence of the background intensity (open circles) and the applied power P (solid triangles) at V_{gs} = −20 V. (e) The background intensity *vs* P at V_{gs} = −20 V. The broken line is the fitting curve calculated by using Planck's law and the Stefan−Boltzmann law for blackbody radiation. The observed background intensity can be fitted with an offset (blue broken circle). (f) EL spectra at V_{gs} = −20 V and V_{ds} = 18 and 28 V. The broken line is the Gaussian peak as a guide to the eye.

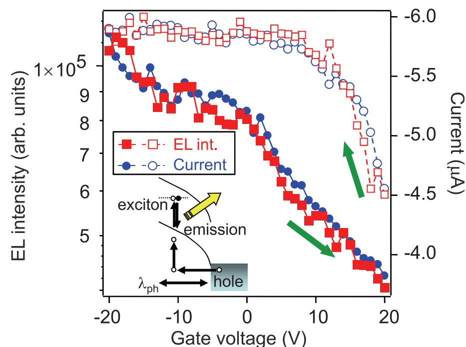

Figure 3. V_{gs} dependence of I_{ds} (blue solid and open circles) and EL intensity (red solid and open squares) at V_{ds} = −23 V for the p-type unipolar device. The positive (solid squares and circles) and negative (open squares and circles) sweep direction of V_{gs} is indicated by arrows. The inset shows the schematics of the impact excitation mechanism.

We also measured the V_{gs} dependence of I_{ds} and the EL intensity at a high bias voltage of V_{ds} = −23 V to investigate the correlation between carrier type and EL intensity (Figure 3). Because our devices exhibit a strong hysteresis during a gate voltage sweep maybe due to trapping and detrapping of impurity states at the surface of the SiO_2 layer,[34,35] the EL spectra and I_{ds} were measured under a sweep to positive (from −20 to 20 V) and negative (from 20 to −20 V) V_{gs}, which enhances n- and p-type regions in V_{gs} dependence, respectively. I_{ds} decreases with increasing V_{gs}; that is, this device exhibits a p-type unipolar characteristic. However, although the current reaches zero at a positive V_{gs} under low bias voltage (as shown in Figure 1b), a finite current remains at a positive V_{gs} under high bias voltage. This is because the height and width of the Schottky barriers for holes are quite low due to applying high bias voltage, and the thermionic and tunneling current flows through the Schottky barriers in all V_{gs} ranges. From the results shown in Figure 3, the V_{gs} dependence of the EL behaves similarly to that of the exponential of the current, and the EL intensity depends on the density of majority carriers (holes in this case).

We now discuss the excitation mechanism of this EL. In early reports of EL, the EL emission caused by: (i) the electron and hole injection mechanism, in which recombination of electrons and holes injected from the opposite electrodes causes the EL emission, was demonstrated.[1−3,7] In this mechanism, however, the emission intensity is proportional to the minority carrier density;[1] therefore, the EL emission obtained in Figure 2 is unlikely to be due to the electron and hole injection mechanism because the behavior of the EL intensity in Figure 3 corresponds to that of the majority carrier density. The other mechanisms, which depend on the majority carrier density, were previously proposed: (ii) the impact excitation and (iii) the thermal excitation mechanisms. In the thermal excitation mechanism, Joule heating and electron scattering by hot optical phonons causes significant electron heating,

and this heating gives rise to a thermal distribution of electrons and holes, which radiatively recombine.[10,11] In this mechanism, the negative differential conductance (NDC) caused by the electron scattering is observed, followed by the EL emission at higher bias voltage. However, although our device in Figure 2b starts to emit EL at V_{ds} = 11 V, NDC is not observed around this bias voltage, where I_{ds} linearly increases as increasing V_{ds}. In addition, although it was previously reported that the light emission of thermal excitation exhibits exponential dependence on power dissipation $P(= I_{ds}V_{ds})$ in a device,[10] the EL intensity shown in Figure 2b does not correlate with the P behavior. Therefore, the thermal excitation mechanism is unlikely to be the dominant mechanism of the observed EL emission.

It is reasonable that the observed EL results from the impact excitation mechanisms (Figure 3, inset), in which the EL intensity exhibits exponential dependence on current as experimentally[4] and theoretically[19−21] demonstrated in previous reports. In the simple model of this mechanism, the emission intensity should be proportional to the impact excitation rate $\exp(-\varepsilon_{th}/\varepsilon)$, where ε is the electric field and ε_{th} (roughly given by $1.5E_g/\lambda_{ph}$, where E_g is the band gap energy and λ_{ph} is the optical phonon scattering length) is the threshold electrical field for impact excitation.[4,19] Because ε_{th} becomes large for a wide band gap nanotube, a high electric field ε is necessary to obtain the short-wavelength EL emission. In our experiment, we obtained the short-wavelength EL emission from a CNFET by applying high bias voltage, which causes an increase in the electric field in a nanotube. As shown in Figure 2b, the curves of the bias voltage dependence of I_{ds} and the emission intensity are shifted to higher bias voltages at V_{gs} = 0 V compared with the curves at V_{gs} = −20 V. These results can be explained by the reduction of band bending in the vicinity of the Schottky contact, taking into account the impact excitation mechanism.[4] At V_{gs} = 0 V, the Schottky barrier height and width for holes become large compared with those at the negative gate voltage, and the bias voltage needed for hole injection becomes large. In addition, the reduction of band bending decreases the electric field in a nanotube in the vicinity of the contacts, and the bias voltage needed for impact excitation increases. (We note that Adam *et al*. distinguished electron−hole injection and impact excitation by observing the position of the emission spot using emission two-dimensional (2D) images;[7] however, the gap of electrodes in our device is too narrow to observe the position of the emission spot between electrodes.)

We also discuss the background of the EL spectra, which increases with increasing V_{ds} in Figure 2a. As shown in Figure 2d, there is some correlation between the background intensity at 0.86 eV (1.45 μm) and the total power dissipation P. Here we fit this result to the curve calculated by using Planck's law and the Stefan−Boltzmann law for blackbody radiation, assuming that the total power from a blackbody radiator is proportional to the applied power P (Figure 2e). The observed background intensity can be explained by the fitted curve with an offset; that is, the observed background increase in Figure 2a is ascribed to the blackbody radiation from the device. From this fitting, the device temperature T at each V_{ds} can be estimated. For example, the maximum T is ∼1390 K at V_{ds} = 28 V, which is consistent with the previously reported temperature obtained from the blackbody radiation of carbon nanotube devices.[36−38] This indicates that the oxygen-absent condition and an unsuspended SWNT are effective in clearly observing the short-wavelength EL at high bias voltage because the heating damage in SWNTs and the blackbody radiation induced by current heating should be prevented.[39] At the low P in Figure 2e, the offset component, which quickly rises at low P (low bias voltage), is observed; however, the origins of this offset remain unclear, and further investigation is needed.

As mentioned above, the emission peak has an unsymmetrical shape with a tail toward the higher energy side (Figure 2f). In addition, the intensity of this tail increases with increasing V_{ds}. (This tail increase also causes a slight shift of peak energy of the EL emission.) This higher energy tail is unlikely to be explained by the binding energy of excitons because the energy broadening of the tail is smaller than the exciton binding energy ($E_b \sim 0.2$ eV for $d \approx 1.0$ nm).[40] This higher energy tail, which increases with V_{ds}, can be explained by: (i) the bound exciton wave function mixing with the band-to-band continuum due to the high electric field[41,42] and (ii) the emission of the thermally excited excitons.[43] The effect of (i) due to the high electric field was theoretically calculated in ref 41, in which the high electric field causes the exciton wave function to mix with the band-to-band continuum that leads to spectral weight transfer from the excitonic peak to the continuum. Moreover, the experimental results of the higher energy broadening of the EL emission peak under the impact excitation condition were explained by this mechanism.[42] In accordance with this mechanism, the increase of the higher energy tail with V_{ds} is caused by spectral weight transfer from the excitonic peak to the continuum due to the high electric field. In addition, the high device temperature increases the higher energy emission because the carriers are thermally activated to the mixed state at high temperature. On the other hand, in the (ii) mechanism, thermally activated excitons occupying the higher energy exciton level contribute to the EL emission at high temperature. In accordance with this mechanism, the blue shift of the EL emission peak in metallic SWNT at high temperature was explained in ref 43. In addition, thermally activated excitons with $K \neq 0$ due to high

device temperature also might be able to contribute to the higher energy emission due to satisfaction of the momentum conservation with phonon assistance. To distinguish the above effects (i) and (ii), further investigation is necessary. For example, the PL measurement at high temperature is useful in investigating the thermal effect. However, blackbody radiation from ambient matter, such as a substrate, should be suppressed to clearly observe emission peaks from a CNT; the current heating is therefore an effective method to investigate the exciton behavior at high temperature because only a CNT can be heated.

The previous report by V. Perebeinos *et al.*[21] theoretically pointed out two competing mechanisms that lead to light emission in SWNT devices: the thermal effect and the impact excitation due to a high electric field. It is an outstanding question as to whether these two competing mechanisms can explain the experimentally obtained light emission. The exciton production rate P is given by the following equation:

$$P = P_0 \exp\left(-\frac{E_{th}}{\sqrt{(k_B T_{op})^2 + (eF\lambda_{op})^2}}\right) \quad (1)$$

where P_0 is a constant and F is the electric field in the SWNTs. The optical phonon temperature $T_{op} \approx T$ is estimated from the fitting of blackbody radiation shown in Figure 2e. $E_{th} \approx 1.22$ (eV nm)/d and $\lambda_{op} \approx 14 \times d$ are the impact excitation threshold energy and the optical phonon mean free path, dependent on the diameter d (~1.0 nm in this device) of the SWNT, respectively.[21] Eq 1 indicates that the exciton production rate is dominated not only by the electric field but also by the temperature and that their contribution to the exciton production rate can be evaluated by comparison between the energy term of k_BT and $eF\lambda_{op}$.[11] We fit the V_{ds} dependence of the emission intensity at $V_g = -20$ V (shown in Figure 2b) using eq 1 and $F \approx \alpha V_{ds}$ as a fitting parameter on the assumption that the emission intensity is proportional to the excitation rate (Figure 4a).[42] The experimental result is well-explained by assuming $\alpha \sim (1.5 \times 10^{-6})^{-1}$. From this fitting, the applied electric field of this device is estimated to be approximately three times smaller than the simple model of the electric field $F_{max} \approx V_{ds}/t_{ox}$, that is, $\alpha \approx (3t_{ox})^{-1}$, where t_{ox} is the gate oxide thickness.[44] This smaller electric field might be due to the thicker gate oxide, which causes the reduction in the screening effect. To evaluate the contribution of impact excitation and the thermal effect, the thermal term energy term k_BT, the impact excitation term $eF\lambda_{op}$, and their ratio ($eF\lambda_{op}/k_BT$) are shown in Figure 4b. Although the ratio of $eF\lambda_{op}/k_BT$ has a constant value of 1.4 at V_{ds} below the EL threshold voltage, the impact excitation term increases with increasing V_{ds} above the threshold voltage (the $eF\lambda_{op}$ term rises to 2.3 times as large as the k_BT term at V_{ds} = 28 V). This increase

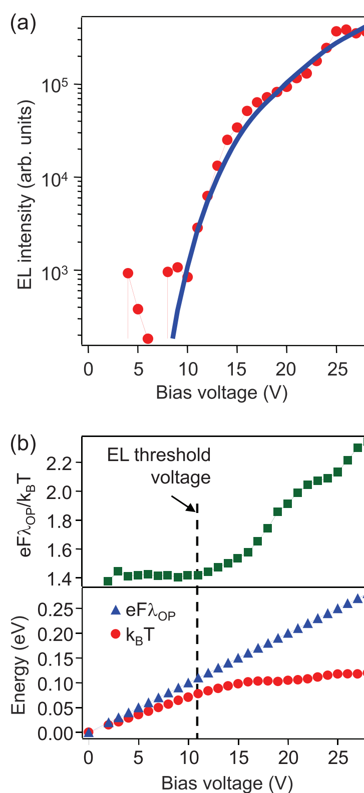

Figure 4. (a) Fitting curve (solid blue line) for the V_{ds} dependence of the EL intensity (red solid circles) at V_{gs} = −20 calculated by using eq 1 and $F \approx \alpha V_{ds}$ as a fitting parameter on the assumption that the emission intensity is proportional to the excitation rate. (b) V_{ds} dependence of the thermal energy term k_BT, the impact excitation term $eF\lambda_{op}$, and their ratio $eF\lambda_{op}/k_BT$. The threshold voltage of the EL emission is indicated by the black broken line.

indicates that the impact excitation makes a major contribution to the EL emission and that the contribution of the thermal effect is small (but not zero). The increase in $eF\lambda_{op}/k_BT$ at high V_{ds} is due to the saturation of the device temperature at high V_{sd}, which results from the current saturation.

In this study, we also observed the short-wavelength EL from the ambipolar CNFETs shown in Figure 1c. Figure 5a shows the EL spectra from the ambipolar CNFET at V_{gs} = 0 V. The EL emission peak appears at ~1.24 eV (~1.0 μm), which is consistent with emission energy estimated from $d \sim 0.9$ nm measured by AFM, and the intensity increases with increasing bias voltage. The V_{ds} dependence of I_{ds} and the EL intensity at V_{gs} = 0 V are shown in Figure 5b. This $I_{ds}-V_{ds}$ characteristic exhibits nearly ohmic behavior in contrast with the p-type CNFET (Figure 2b) due to the lower Schottky barriers at V_{gs} = 0 V. In contrast, the EL intensity drastically increases over the threshold V_{ds} of ~11.5 V. To determine the excitation mechanism of this emission, the correlation between carrier type and emission intensity was investigated by measuring the V_{gs} dependence of I_{ds} and the EL intensity at V_{ds} = −10 V (Figure 5c). I_{ds} increases in both regions of the negative (p-type) and positive (n-type) V_{gs}; that is, the

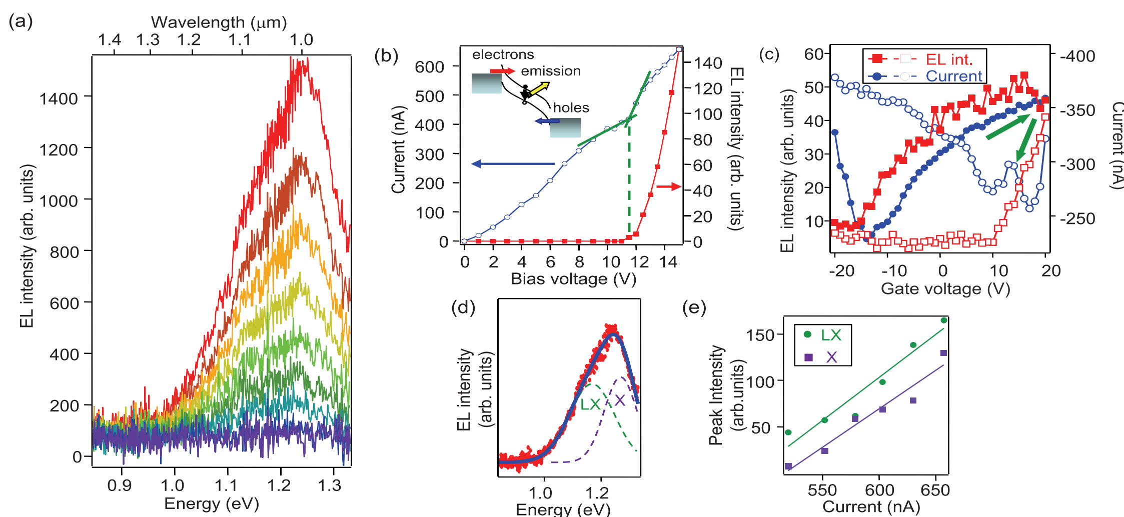

Figure 5. (a) EL spectra from the ambipolar device as a function of V_{ds} at V_{gs} = 0 V and V_{ds} = 11−15 V with steps of 0.5 V. (b) V_{ds} dependence of I_{ds} (blue open circles) and the EL intensity (red solid squares) at V_{gs} = 0 V. The inset shows the schematics of the electron and hole injection mechanism. At a threshold voltage of EL (green broken line), the slope of the I_{ds}−V_{ds} curve suddenly increases (green solid lines). (c) V_{gs} dependence of I_{ds} (blue solid and open circles) and EL intensity (red solid and open squares) at V_{ds} = −10 V. The positive (solid squares and circles) and negative (open squares and circles) sweep direction of V_{gs} is indicated by the arrows. (d) Two Gaussian fittings for the EL spectrum at V_{gs} = 0 V and V_{ds} = 15 V. X (purple broken line) and LX (green broken line) peaks are assigned to the free exciton and weakly localized exciton emission, respectively. (e) Current dependence of the X and LX integrated peak intensity. Linear fittings for X and LX are also indicated by solid lines.

ambipolar characteristic is preserved at high V_{ds}. On the other hand, the EL intensity is increased only in the n-type (the positive V_{gs}) region and is suppressed in the p-type (the negative V_{gs}) region. This result indicates that the EL intensity does not depend on the current value but on the electron density. As mentioned above, the EL intensity depends on the density of majority carriers for the EL of the impact excitation[4] and thermal excitation mechanisms;[10] therefore, the observed emission of Figure 5 is unlikely to be explained by these excitation mechanisms.

The possible excitation mechanism of the EL dominated by the minority carriers is the electron and hole injection (Figure 5b, inset).[1−3,7] In this mechanism, electrons behave as minority carriers because the EL intensity, which is dominated by the density of minority carriers, increases in the n-type region. In the simple model of this mechanism, the EL intensity is proportional to the product of minority and majority carrier densities. Therefore, to explain the V_{gs} dependence of I_{ds} and the EL intensity in Figure 5c, the hole density should be sufficiently high in all gate voltage ranges, and the electrons should be suppressed in the negative gate voltage ranges because the EL emission is observed only in the n-type region. This is because the Schottky barrier height for holes is greatly decreased by applying high bias voltage. The current exhibits the ambipolar characteristic (*i.e.*, current increases as increasing negative and positive gate voltages), as shown in Figure 5c, because the current is dominated by the sum of the electron and hole density. In fact, in contrast to the V_{gs} dependence at low bias voltage shown in Figure 1b, I_{ds} is not suppressed between the n- and p-type regions in Figure 5c because the high bias voltage allows hole injection throughout the gate voltage range. In addition, this mechanism of electron and hole injection explains the current and EL intensity change at the threshold bias voltage of the V_{ds} dependence result. As shown in Figure 5b, the slope of the I_{ds}−V_{ds} curve suddenly increases at the threshold voltage of EL. This increase is due to the electron injection being increased at the threshold voltage in response to the reduction in the Schottky barrier height for electrons by applying high bias voltage. The device begins to emit at this V_{ds} by recombination of the injected minority carriers of the electrons and the majority carriers of holes.

The EL emission peaks in Figure 5a are asymmetric, and the emission profiles can be fitted by two Gaussians (Figure 5d). Given the similar splitting previously observed in the EL from a SWNT diode,[42] the higher and lower emission peaks can be assigned to the free exciton (X) and weakly localized exciton (LX) emission, respectively. The exciton localization might be due to environmental fluctuation or brightening of intrinsic dark states at structural defect sites.[42] In addition, as shown in Figure 5e, the current dependence of X and LX peak intensity exhibits the same slope. This is also consistent with the previous observation in a SWNT diode,[42] although the LX intensity is not saturated because the number of excitons is insufficient to occur Auger-mediated exciton−exciton annihilation.

In conclusion, we have measured EL for the CNFETs with unsuspended SWNTs in high vacuum, and short-wavelength EL emission was observed from unipolar and ambipolar CNFETs under high bias voltage. The

simultaneous measurements of transport and EL spectra reveal the excitation mechanism of impact excitation or electron and hole injection dependent on the conduction type of unipolar or ambipolar characteristics. Short-wavelength emission under high bias voltage is due to the Schottky barrier reduction and the electric field increase in a SWNT. Blackbody radiation is also observed from the CNFETs due to current heating. To clearly observe short-wavelength EL at high bias voltage, the oxygen-absent condition and an unsuspended SWNT are effective because the oxidation damage and the blackbody radiation due to current heating should be prevented. Using the device temperature estimated from blackbody radiation, the contribution of impact excitation and thermal effect to the exciton production rate was evaluated. Short-wavelength EL should make it possible to use optical fibers and Si detectors; the SWNT light-emitting device is therefore expected to be used as the microlight source in optical communication and other optical applications.

METHODS

CNFETs were fabricated using electron beam (EB) lithography and lift-off processes on a heavily doped p-type Si substrate with a thermally oxidized SiO_2 layer of 500 nm thickness. SWNTs were grown by chemical vapor deposition using ethanol from the Co catalysts, which were patterned with a size of 10×10 μm^2.[45] Source and drain electrodes of 30 nm Pd metal were formed on a SWNT with a gap of 5 μm, and a single SWNT was contacted to the electrodes (Figure 1a). Gate voltage (V_{gs}) was applied through the substrate as a back gate. The electric properties of the devices were measured as a function of the drain source bias voltage (V_{ds}) and V_{gs} at room temperature in a high-vacuum chamber ($<10^{-6}$ Torr), which prevents current-induced oxidation. EL spectra were also measured at room temperature in high vacuum. In the EL measurement, the emission light was passed through a quartz optical window of the chamber and a microscope objective. The EL spectra were acquired using a spectrometer and an InGaAs detector. The relative spectral response of the measurement system including the optical path and the detector was measured by a calibrated halogen lamp, and all spectra were corrected accordingly. To investigate the EL mechanisms, the electrical and EL measurements were carried out simultaneously.

Acknowledgment. This work was partially supported by Grants-in-Aid for the Encouragement of Young Scientists (grant no. 20740177) from the Ministry of Education, Culture, Sports, Science, and Technology of Japan, by the TEPCO Research Foundation and by the Strategic Information and Communications R&D Promotion Program (SCOPE, no. 082103001) of the Ministry of Internal Affairs and Communications of Japan.

REFERENCES AND NOTES

1. Misewich, J. A.; Martel, R.; Avouris, P.; Tsang, J. C.; Heinze, S.; Tersoff, J. Electrically Induced Optical Emission from a Carbon Natotube FET. *Science* **2003,** *300*, 783.
2. Freitag, M.; Chen, J.; Tersoff, J.; Tsang, J. C.; Fu, Q.; Liu, J.; Avouris, P. Mobile Ambipolar Domain in Carbon-Nanotube Infrared Emitters. *Phys. Rev. Lett.* **2004,** *93*, 07803.
3. Freitag, M.; Perebeinos, V.; Chen, J.; Stein, A.; Tsang, J. C.; Misewich, J. A.; Martel, R.; Avouris, P. Hot Carrier Electroluminescence from a Single Carbon Nanotube. *Nano Lett.* **2004,** *4*, 1063.
4. Chen, J.; Perebeinos, V.; Freitag, M.; Tsang, J.; Fu, Q.; Liu, J.; Avouris, P. Bright Infrared Emission from Electrically Induced Excitons in Carbon Nanotubes. *Science* **2005,** *310*, 1171.
5. Freitag, M.; Tsang, J. C.; Kirtley, J.; Carlsen, A.; Chen, J.; Troeman, A.; Hilgenkamp, H.; Avouris, P. Electrically Excited, Localized Infrared Emission from Single Carbon Nanotubes. *Nano Lett.* **2006,** *6*, 1425.
6. Xia, F.; Steiner, M.; Lin, Y.; Avouris, P. A Microcavity-Controlled, Current-Driven, On-Chip Nanotube Emitter at Infrared Wavelengths. *Nat. Nanotechnol.* **2008,** *3*, 609.
7. Adam, E.; Aguirre, C. M.; Marty, L.; St-Antoine, B. C.; Meunier, F.; Desjardins, P.; Ménard, D.; Martel, R. Electroluminescence from Single-Walled Carbon Nanotube Network Transistors. *Nano Lett.* **2008,** *8*, 2351.
8. Marty, L.; Adam, E.; Albert, L.; Doyon, R.; Menard, D.; Martel, R. Exciton Formation and Annihilation during 1D Impact Excitation of Carbon Nanotubes. *Phys. Rev. Lett.* **2006,** *96*, 136803–1.
9. Essig, S.; Marquardt, C. W.; Vijayaraghavan, A.; Ganzhorn, M.; Dehm, S.; Hennrich, F.; Ou, F.; Green, A. A.; Sciascia, C.; Bonaccorso, F.; Bohnen, K.-P.; von Loehneysen, H.; Kappes, M. M.; Ajayan, P. M.; Hersam, M. C.; Ferrari, A. C.; Krupke, R. Phonon-Assisted Electroluminescence from Metallic Carbon Nanotubes and Graphene. *Nano Lett.* **2010,** *10*, 1589.
10. Mann, D.; Kato, Y. K.; Kinkhabwala, A.; Pop., E.; Cao., J.; Wang, X.; Zhang, L.; Wang., Q.; Guo, J.; Dai, H. Electrically Driven Thermal Light Emission from Individual Single-Walled Carbon Nanotubes. *Nat. Nanotechnol.* **2007,** *2*, 33.
11. Wang, X.; Zhang, L.; Lu, Y.; Dai, H.; Kato, Y. K.; Pop., E. Electrically Driven Light Emission from Hot Single-Walled Carbon Nanotubes at Various Temperatures and Ambient Pressures. *Appl. Phys. Lett.* **2007,** *91*, 261102.
12. Bachilo, S. M.; Strano, M. S.; Kittrell, C.; Hauge, R. H.; Smalley, R. E.; Weisman, R. B. Structure-Assigned Optical Spectra of Single-Walled Carbon Nanotubes. *Science* **2002,** *298*, 2361.
13. O'Connell, M. J.; Bachilo, S. M.; Huffman, C. B.; Moore, V. C.; Strano, M. S.; Haroz, E. H.; Rialon, K. L.; Boul, P. J.; Noon, W. H.; Kittrell, C.; Ma, J.; Hauge, R. H.; Weisman, R. B.; Smalley, R. E. Band Gap Fluorescence from Individual Single-Walled Carbon Nanotubes. *Science* **2002,** *297*, 593.
14. Lefebvre, J.; Homma, Y.; Finnie, P. Bright Band Gap Photoluminescence from Unprocessed Single-Walled Carbon Nanotubes. *Phys. Rev. Lett.* **2003,** *90*, 217401.
15. Hartschuh, A.; Pedrosa, H. N.; Novotny, L.; Krauss, T. D. Simultaneous Fluorescence and Raman Scattering from Single Carbon Nanotube. *Science* **2003,** *301*, 1354.
16. Lebedkin, S.; Hennrich, F.; Skipa, T.; Kappes, M. M. Near-Infrared Photoluminescence of Single-Walled Carbon Nanotubes Prepared by the Laser Vaporization Method. *J. Phys. Chem. B* **2003,** *107*, 1949.
17. Matsuda, K.; Kanemitsu, Y.; Irie, K.; Saiki, T.; Someya, T.; Miyauchi, Y.; Maruyama, S. Photoluminescence Intermittency in an Individual Single-Walled Carbon Nanotube at Room Temperature. *Appl. Phys. Lett.* **2005,** *86*, 123116.
18. Chen, Z.; Appenzeller, J.; Knoch, J.; Lin, Y.; Avouris, P. The Role of Metal-Nanotube Contact in the Performance of Carbon Nanotube Field-Effect Transistors. *Nano Lett.* **2005,** *5*, 1497.
19. Guo, J.; Alam, M. A.; Ouyang, Y. Subband Gap Impact Ionization and Excitation in Carbon Nanotube Transistors. *J. Appl. Phys.* **2007,** *101*, 064311.
20. Koswatta, S. O.; Perebeinos, V.; Lundstrom, M. S.; Avouris, P. Computational Study of Exciton Generation in Suspended Carbon Nanotube Transistors. *Nano Lett.* **2008,** *8*, 1596.

21. Perebeinos, V.; Avouris, P. Impact Excitation by Hot Carriers in Carbon Nanotubes. *Phys. Rev. B: Condens. Matter Mater. Phys.* **2006,** *74*, 121410.
22. Collins, P. G.; Arnold, M. S.; Avouris, P. Engineering Carbon Nanotubes and Nanotube Circuits Using Electrical Breakdown. *Science* **2001,** *292*, 706.
23. Collins, P. G.; Hersam, M.; Arnold, M. S.; Martel, R.; Avouris, P. Current Saturation and Electrical Breakdown in Multiwalled Carbon Nanotubes. *Phys. Rev. Lett.* **2001,** *86*, 3128.
24. Radosavljević, M.; Lefebvre, J.; Johnson, A. T. High-Field Electrical Transport and Breakdown in Bundles of Single-Wall Carbon Nanotubes. *Phys. Rev. B: Condens. Matter Mater. Phys.* **2001,** *64*, 241307.
25. Pop, E.; Mann, D. A.; Goodson, K. E.; Dai, H. Electrical and Thermal Transport in Metallic Single-Wall Carbon Nanotubes on Insulating Substrates. *J. Appl. Phys.* **2007,** *101*, 093710.
26. Tans, S. J.; Verschueren, A; Dekker, C. Room-Temperature Transistor Based on a Single Carbon Nanotube. *Nature* **1998,** *393*, 49.
27. Javey, A.; Guo, J.; Wang, Q; Lundstrom, M; Dai, H. Ballistic Carbon Nanotube Field-Effect Transistors. *Nature* **2003,** *424*, 654.
28. Moon, S.; Lee, S.; Song, W.; Lee, J. S.; Kim, N.; Kima, J.; Park, N. Fabrication of n-type Nanotube Transistors with Large-Work-Function Electrodes. *Appl. Phys. Lett.* **2007,** *90*, 092113.
29. Aguirre, C. M.; Levesque, P. L.; Paillet, M.; Lapointe, F.; St-Antoine, B. C.; Desjardins, P.; Martel, R. The Role of the Oxygen/Water Redox Couple in Suppressing Electron Conduction in Field-Effect Transistors. *Adv. Mater.* **2009,** *21*, 3087.
30. Martel, R.; Derycke, V.; Lavoie, C.; Appenzeller, J.; Chan, K. K.; Tersoff, J.; Avouris, Ph. Ambipolar Electrical Transport in Semiconducting Single-Wall Carbon Nanotubes. *Phys. Rev. Lett.* **2001,** *87*, 256805.
31. Weisman, R. B.; Bachilo, S. M. Dependence of Optical Transition Energies on Structure for Single-Walled Carbon Nanotubes in Aqueous Suspension: An Empirical Kataura Plot. *Nano Lett.* **2003,** *3*, 1235.
32. Yao, Z.; Kane, C. L.; Dekker, C. High-Field Electrical Transport in Single-Wall Carbon Nanotubes. *Phys. Rev. Lett.* **2000,** *84*, 2941.
33. Pop, E.; Mann, D.; Cao, J.; Wang, Q.; Goodson, K.; Dai, H. Negative Differential Conductance and Hot Phonons in Suspended Nanotube Molecular Wires. 2005. *Phys. Rev. Lett.* **2005,** *95*, 155505.
34. Fuhrer, M. S.; Kim, B. M.; Dürkop, T.; Brintlinger, T. High-Mobility Nanotube Transistor Memory. *Nano Lett.* **2002,** *2*, 755.
35. Radosavljevic, M.; Freitag, M.; Thadani, K. V.; Johnson, A. T. Nonvolatile Molecular Memory Elements Based on Ambipolar Nanotube Field Effect Transistors. *Nano Lett.* **2002,** *2*, 761.
36. Li, P.; Jiang, K.; Liu, M.; Li, Q.; Fan, S. Polarized Incandescent Light Emission from Carbon Nanotubes. *Appl. Phys. Lett.* **2003,** *82*, 1763.
37. Sveningsson, M.; Jönsson, M.; Nerushev, O. A.; Rohmund, F.; Campbell, E. E. B. Blackbody Radiation from Resistively Heated Multiwalled Carbon Nanotubes During Field Emission. *Appl. Phys. Lett.* **2002,** *81*, 1095.
38. Wei, J.; Zhu, H.; Wu, D.; Wei, B. Carbon Nanotube Filaments in Household Light Bulbs. *Appl. Phys. Lett.* **2004,** *84*, 4869.
39. Lefebvre, J.; Austing, D. G.; Finnie, P. Two Modes of Electroluminescence from Single-Walled Carbon Nanotubes. *Phys. Status Solidi RRL* **2009,** *3*, 199.
40. Perebeinos, V.; Tersoff, J.; Avouris, P. Scaling of Excitons in Carbon Nanotubes. *Phys. Rev. Lett.* **2004,** *92*, 257402.
41. Perebeinos, V.; Avouris, P. Exciton Ionization, Franz-Keldysh, and Stark Effects in Carbon Nanotubes. *Nano Lett.* **2007,** *7*, 609.
42. Mueller, T.; Kinoshita, M.; Steiner, M; Perebeinos, V.; Bol, A. A.; Farmer, D. B.; Avouris., P. Efficient Narrow-Band Light Emission from a Single Carbon Nanotube p-n Diode. *Nat. Nanotechnol.* **2010,** *5*, 27.
43. XIe, L.; Farhat, H.; Son, H.; Zhang, H.; Dresselhaus, M. S.; Kong, J.; Liu, Z. Electroluminescence from Suspended and On-Substrate Metallic Single-Walled Carbon Nanotubes. *Nano Lett.* **2009,** *9*, 1747.
44. Heinze, S.; Radosavljevic, M.; Tersoff, J.; Avouris, Ph. Unexpected Scaling of the Performance of Carbon Nanotube Schottky-Barrier Transistors. *Phys. Rev. B: Condens. Matter Mater. Phys.* **2003,** *68*, 235418.
45. Maki, H.; Mizuno, T; Suzuki, S.; Sato, T; Kobayashi, Y. Multi-Back-Gate Control of Carbon Nanotube Double-Quantum Dot. *Jpn. J. Appl. Phys.* **2009,** *48*, 04C201.